RSC Advances

ROYAL SOCIETY OF CHEMISTRY

www.rsc.org/advances

Graphical Abstract

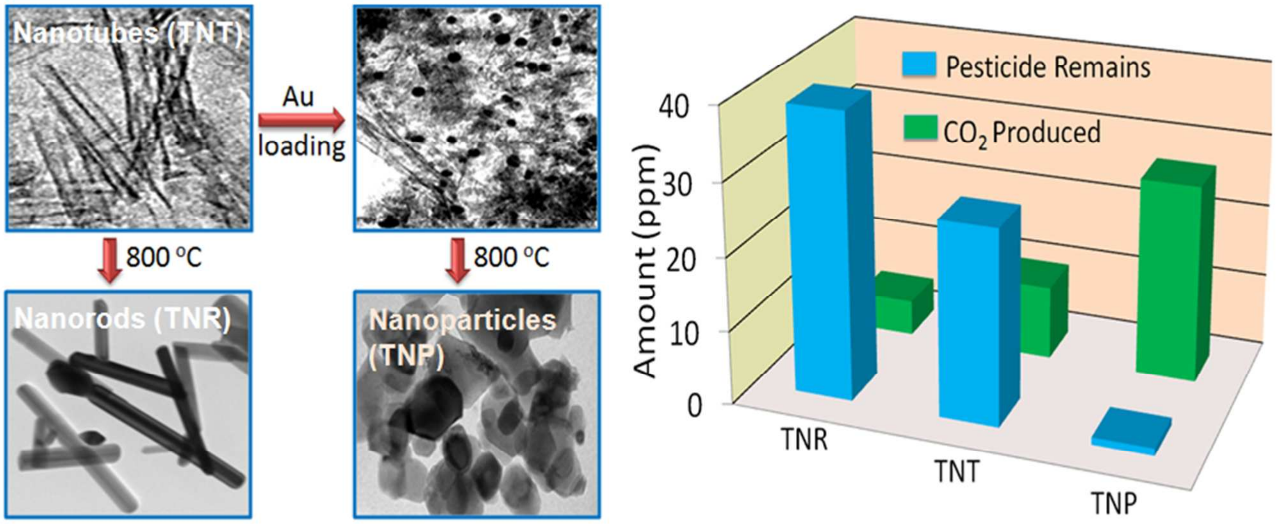

Title: Influence of thermal treatment and Au-loading on the growth of versatile crystal phase composition and photocatalytic activity of sodium titanate nanotubes

Author's name: Inderpreet Singh Grover, Satnam Singh and Bonamali Pal*

Designation: First author is Ph.D. student, second author is Associate Professor and third author is Professor .

Address:
School of Chemistry and Biochemistry,
Thapar University,
Patiala 147004,
Punjab (India)

Corresponding author:
Bonamali Pal
E-mail: bpal@thapar.edu
Tel: 91-175-2393128

Fax: 91-175-2364498

Abstract: A coalescence influence of Au-loading followed by calcination at 800 ^{o}C led to a notable change in crystal-structure, morphology, phase composition and photocatalytic activity of titanate-nanostructures. After calcination at 800 ^{o}C, bare sodium titanate nanotubes (TNT) having BET surface area (S_{BET}) of 176 m^2g^{-1} is transformed to sodium titanate nanorods of S_{BET} = 21 m^2g^{-1}, whereas calcination of Au-loaded (Au^{+3}, Au^{o} and Au-nanoparticle (AuNP)) TNT at 800 ^{o}C led to a variety of fragmented particles having different crystal structures, S_{BET} (21-39 m^2g^{-1}), shape and sizes (50-75 nm), attributed to strain induced thermal decomposition of TNT after Au-loading, and the oxidation state of Au is determined by XPS analysis. The comparative photocatalytic activitiy of these as-prepared catalysts to that of P25-TiO_2 under UV-light were evaluated for the photooxidation of insecticide imidacloprid which gradually degraded to various intermediate photoproducts and finally decomposes to CO_2. The degradation of imidacloprid follows pseudo-first order kinetics, where 0.5 wt% Au^{o}-deposited-TNT after calcination exhibits highest photocatalytic activity (rate constant $k = 8.9 \times 10^{-3}$ min^{-1}), which are comparatively explained on the basis of their crystal phase, surface-area, morphology and relaxation time of photoexcited electron-hole pairs, as measured by time resolved spectroscopy.

Keywords: Na-titanate nanostructures, Photoactivity of Au-titanates, Alkali metal titanates, Effect of calcination on titanates, Crystal phases of Na-titanates

1 Introduction

Sodium titanate nanotubes having layered structure, hollow-porous morphology and higher surface area, generally exhibit flexible photocatalytic activity (PCA) depending (1-6) upon the sodium content, crystal phase, and calcination temperature. Systematic studies of TNT with moderate Na content on the thermal treatment at 200 to 900 ^{o}C revealed that it retains its tubular morphology when calcined at 200-450 ^{o}C, indicating its thermal stability in this temperature range and showing higher photocatalytic activity (1,5) than the mostly active P25-TiO_2 (P25) photocatalyst. However, with further increase in calcination temperature to ~ 700-800 ^{o}C, the hollow interior of TNT collapse through the condensation of edge sharing TiO_6 coggurated layers resulting in rigid and solid sodium titanate nanorods (TNT(C)) showing almost similar photoactivity (7,8) to P25 catalyst.

The PCA of TNT was further enhanced (9-13) by impregnation with transition metals (Fe, Ni, Pt, Au, Ru etc.) followed by calcination at 200-450 ^{o}C. It has been reported (9,11,12,14) that incorporation of metals (Fe, Au, Ni) into hollow interior of TNT facilitated the formation of core-shell structure with improvement in the lifetime of photoexcited e^-/h^+ pair, hence the photocatalytic activity. For instance, in comparison to bare TNT, Fe and Au incorporated TNT were reported (11,12) to be 5.0 and 7.6 times more photoactive toward the photooxidation of CO and H_2 production, respectively, where no significant change in either morphology or crystal structure was observed. However, the effect of these impregnated metals in TNT after calcinations > 450 ^{o}C have been rarely reported, and is expected (15,16) to cause deformations in crystal structure/morphology during calcination. The metal may induce a strain in the crystal structure (15) or decrease the surface free energy (16) of TNT that may interfere with its crystal growth during calcination. Very recently, a report by Portai et al. (17) demonstrated that calcination of Rh deposited TNT at 600 °C led to the formation of nanoparticles of size ~ 10 nm, instead of any elongated morphology like solid nanorods (1-6) i.e., TNT(C) formed during calcination of bare TNT. In this context, present work demonstrates that calcination of Au photodeposited Au^{+3} and Au nanospheres (3-5 nm) impregnated TNT under atmospheric conditions at ~ 800 °C for 2 h resulted in the formation of a variety of geometrical morphologies e.g., nanopolygons like heptagons, hexagons, pentagons, etc. These nanoparticles were found to possess different crystal structures (monoclinic, orthorhombic and rhombohedral) and phase compositions in comparison to monoclinic TNT(C) particles that were obtained after calcination of monoclinic TNT without Au loading, under similar conditions. The formation of versatile crystal geometries, allowed exploring the crystal phase dependent photocatalytic activity relative to the mostly studied anatase, anatase-rutile, rutile and brookite TiO_2 phases. Hence, various physicochemical properties of as-prepared titania nanocomposites were briefly investigated for the photooxidation of neurotoxic (18-21) insecticide imidacloprid (IMI) to plausible intermediate products that mineralize to CO_2 under different periods of UV-light irradiation.

2 Experimental

Sodium hydroxide (AR)**,** Methanol (AR), Acetonitirile (HPLC), Isopropyl alcohol (AR), Auric Chloride ($HAuClO_4$. xH_2O) and Nitric acid were purchased from Loba Chemie, India. Commercially available P25-TiO_2 and imidacloprid were obtained from Degussa Corporation, Germany and Ravi Organics Pvt. Ltd. (Mumbai), India, respectively. Standard CO_2 gas (200 ppm) with N_2 gas was obtained from Centurion Scientific Pvt. Ltd, New Delhi, India. All the chemicals were used without further purification.

2.2 Synthesis, characterization and photoactivity of TNT and TNT(C) particles

In a typical experiment, an appropriate amount of P25 was mixed with NaOH (10 M) and autoclaved for 20 h as reported recently by our group (6). The Au nanospheres were prepared by method as decried in our previous report (22).The Au loading was carried out by (i) the addition of 1.2 ml of 0.01 mM aqueous solution of $HAuCl_4.xH_2O$ (0.5 wt% of Au) during the preparation of TNT, designated as TNT-Au^{+3}, and was irradiated in de-aerated 5 ml of 50% v/v aqueous isopropyl alcohol under UV light (125 W Hg arc lamp) for 2 h, as a result Au^{+3} is reduced (6) to Au^{o} and designated as TNT-Au^{o}. (ii) Mixing of TNT (100 mg) with 500 µl spherical Au nanoparticles (NP, size 3-5 nm) in 3 ml of de-ionized water under stirring for 2 h followed by drying, named as TNT-AuNP sample. Bare and Au-loaded TNT were calcined in an alumina crucible at 800 ^{o}C (heating rate 5 ^{o}C/min) for 2 h using muffle furnace (Jupiter Scientific) and are abbreviated as TNT(C) and TNT-Au^{+3}(C), TNT-Au^{o}(C) and TNT-AuNP(C).

All the samples were characterized by absorption spectrophotometer (Ocean Optics 4000USB) and XRD (Panalytical X'-pert using Cu Kα, λ=1.54178 Å). X'Pert HighScore Plus software was used for identification of various crystal structure(s) formed after calcination. Transmission electron microscopy (TEM) images were recorded on Hitachi 7500 electron microscope, using 120 kV accelerating voltage. Samples for TEM analysis were prepared by depositing them onto Cu grid by dropping a drop of methanolic suspension (5mg/ml) on it which was then dried. The elemental detection analysis (EDS) was performed on JEOL JSM-6510LV by fixing them onto Cu grid having double sided adhesive carbon tape. The XPS spectra of as-prepared samples were recorded on Leybold Heraeus-Shengyang SKL-12 electron spectrometer equipped with VG CLAM 4 MCD electron energy analyzer, using Al-Kα as excitation source, for the 4f electrons of Au-only in order to determine its oxidation state. The samples for XPS-analysis were prepared by fixing the fine powdered sample (~50 mg) on the stub having double side-adhesive carbon tape, and the unattached sample to this stub was removed before the XPS analysis. The BET surface area was measured with Smart Sorb 91/92 using 150 mg of sample preheated at 150 ^{o}C for 1 h. Time resolved luminescence decay curves of powder samples were recorded using Nitrogen laser (excitation at 390 nm) pulsed in operation (5-7 ns pulse width) coupled with Tektronix TDS-1012 oscilloscope, where 100 ml of 50 ppm aqueous solution of imidacloprid (IMI, substrate for degradation) and 50 mg of as-prepared TNT-Au^{o}(C) and TNT-AuNP(C) catalysts were stirred for 30 min in dark. The mixture was centrifuged (Remi-3402, 4000 rpm for 4 min), dried (70-80 ^{o}C for 30 min) and denoted as IMI+TNT-Au^{o} (C) and IMI+TNT-AuNP(C) and their time resolve luminescence decay curves were also recorded. Prior to this analysis the samples (10-20 mg) were placed onto quartz stub, 100 µl of methanol was added, dried (70-80 ^{o}C) for 20-30 min in-order to fix the samples on this stub. All physicochemical properties and description for as-prepared nanostructures are listed in Table 1.

The photooxidation of IMI was carried out in a test tube (sealed with rubber cap) containing 5 ml aqueous solution of imidacloprid (50 ppm) and 2.5 mg bare or Au loaded nanocrystals under UV (125 W Hg arc, 10.4 mW/cm^2) irradiation for 3 h. A blank experiment without catalyst was also performed under above experimental conditions to study the photodegradation behavior of IMI only under UV-light. The reaction solution was analyzed by high performance liquid chromatography (HPLC, Agilent 1120LC) using C-18 column (BDS, Qualigens) of dimensions 250 mm × 4.6 mm and particle size of 5 µm with 80:20:: acetonitrile : water as mobile phase at a flow rate of 1 ml/min and detection wavelength of 270 nm. The evolution of CO_2 was determined by injecting 1 ml of gaseous mixture from the reaction vessel (gas tight test tube) into gas chromatogram (NUCON-5765) using Porapak-Q column with nitrogen as carrier gas (30 ml/min) using Thermal Conductivity Detector (TCD). Column oven was maintained at 40 ^{o}C while the injector and detector were kept at 70 and 80 ^{o}C, respectively. Intermediates formed after 3 h of UV-light exposure were identified by injecting 20 µl of reaction sample in LC-MS (Bruker-300PS) having single-quadruple detector, equipped with C-18 column (Hypersil, 150 mm× 4.6 mm, 5 µm) using a mobile phase of 80:20:: acetonitrile : water at a flow rate of 1 ml/min.

3 Results and discussion

The XRD pattern and TEM images for as-prepared TNT and TNT(C) are shown in Fig. 1. It was found that as-prepared TNT possess monoclinic crystal structure for $Na_2Ti_3O_7$ (tritianate) as evidenced (ICSD card no.00-014-0085) by its characteristic peak at $2\theta = 10.0015^{o}$ for (101) plane. The presence of Na in TNT and TNT(C) is confirmed by EDS analysis (*Electronic Supplementary Information (ESI)-fig. 1*) and is in agreement (6,23) with our recent reports. The calcination of bare TNT caused its transformation to nanorods (TNT(C)) particles of orthorhombic $Na_2Ti_6O_{13}$ (hexatitanate) crystal structure. The TEM images of TNT and TNT(C) showed tubular and rod like morphology and their corresponding SAED pattern indicates amorphous and crystalline nature, respectively, are in accordance with their respective XRD pattern.

The XRD pattern, TEM and EDS analysis of TNT-Au^{+3} and TNT-Au^{+3}(C) samples are shown in Fig. 2. It was found that the XRD pattern of TNT-Au^{+3} is almost similar to TNT, whereas, TNT-Au^{+3}(C) was found to composed of a mixture of well crystalline, strained $Na_2Ti_9O_{19}$ (nonatitanate, ICSD Card No. 01-073-2256), $Na_2Ti_6O_{13}$ (hexatitanate) and $NaTiO_2$ (monotitanate, ICSD Card No. 00-016-0251) crystal structures. Interestingly, deviation in lattice parameters (Table 1) and shift in characteristic peaks for nonatitanate ($2\theta = 24.71^{\circ}$ to 24.81°), hexatitanate ($2\theta = 11.84^{\circ}$ to 11.92°), and monotitanate ($2\theta = 40.67^{\circ}$ to 40.72°) were found corresponding to (110), (200) and (104) planes, respectively which might be due to exchange of Na^{+} ions by Au^{+3} ions. For a 6-fold coordinated ion the radius of Na^{+} ions (1.12 Å) is more than radius of Au^{+3} (0.85 Å) ion, hence the exchange of the former with the later ion resulted in compression strain ca. 6.9×10^{-3} in crystal structure of TNT-Au^{+3}, and subsequently causing these variations. The morphology of TNT-Au^{+3}(C) was found to be of nanopolygons, with its SAED pattern exhibiting crystalline nature and is similar to XRD pattern. The presence of Au in TNT-Au^{+3}(C) is further confirmed by EDS analysis (Fig. 2f) where 0.4 wt% of Au was found to be present along with Na (0.5 wt%), Ti (57.6 wt%) and O (41.5 wt%). The measured $S_{BET} = 160$ $m^{2}g^{-1}$ of TNT-Au^{+3} was reduced to 28 $m^{2}g^{-1}$ after its calcinations (TNT-Au^{+3}(C)) that can be ascribed to the formation of highly crystalline nanopolygons particles like morphology.

On the other hand, TNT-Au^{o} found to corresponds to $H_2Ti_3O_7$. H_2O (trititanic acid), while, TNT-Au^{o}(C) is found to be a mixture of anatase and rutile phases, as revealed by the characteristic peaks in their respective XRD patterns as seen in Fig. 3. The formation of trititanic acid instead of trititanate could be attributed to the exchange of Na^{+} ions by the photoproduced H^{+} ions during photodeposition of Au. This H^{+} ions could be replaced (24) easily by Na^{+} ions due to (i) weaker Vander-Walls forces of attraction between Na^{+} with $Ti_3O_7^{-2}$ layers, (ii) longer bond length (2 Å) of Na-O in $Na_2Ti_3O_7.H_2O$ than 1 Å of H-O bond length in $H_2Ti_3O_7.H_2O$, and (iii) lower elution strength of the Na^{+} ions than H^{+} ions favoring their exchange. However, small deviations have been found in lattice parameters for TNT-Au^{o}(C) having anatase (ICDS card number: 00-001-0562) and rutile (ICDS card number: 00-01-1292) phases in comparison to their standard values. This may be due to incorporation of Au^{+3} ions in-between octahedral layers of

TiO_6 in TNT that got exchanged and subsequently deposited during UV-illumination resulting in a strain in the crystal structure and altering the lattice parameters.

The acquired TEM images for morphological analysis of TNT-Au^o and TNT-Au^o (C) are shown in Fig. 3. The deposition of Au-nanoparticles of size 10-15 nm onto TNT can be clearly seen for TNT-Au^o. However, the presence of Au (0.5 wt%) was confirmed by the EDS elemental analysis (Fig. 3d). The TNT-Au^o(C) was found to be composed of fragmented nanocrystals of size 50-60 nm with more number of boat shaped nanoparticles than that found for TNT-Au^{+3}(C). Moreover, the obtained SAED pattern for TNT-Au^o(C) also indicates its high crystallinity and is in conformity with its XRD pattern. The S_{BET} for TNT-Au^o (156 m^2g^{-1}) was ~ 1.2 times less than TNT (176 m^2g^{-1}) and is in accordance with our previous report (6), showing decrease in S_{BET} after photodeposition of Ag and Cu onto TiO_2 nanorods, P25 and TNT. However, S_{BET} = 39 m^2g^{-1} for TNT-Au^o(C) was higher than S_{BET} = 28 m^2g^{-1} for TNT-Au^{+3}(C) that could be rationalized to its small particle size.

The XRD pattern, TEM images of TNT-AuNP, TNT-AuNP(C) and SAED and EDS pattern of TNT-AuNP(C) are shown Fig. 4. The XRD pattern of TNT-AuNP reveals it be composed of monoclinic $Na_2Ti_3O_7$, while TNT-AuNP(C) was found to be a mixture of $Na_2Ti_3O_7$, $Na_2Ti_6O_{13}$ and $NaTiO_2$ crystal structures and well consistent to its ca. lattice parameters to that of reported values (ICSD card no. 01-072-0148 and 01-089-0802) indicating it to be almost strain free. It might be because of negligible probability of exchange of Na^+ ions by AuNP with much larger diameter (3-5 nm). The absence of strain (Table 1) in the crystal structure of TNT-NP sample also supports the assumption that Na^+ ions in TNT-Au^{+3} and TNT-Au^o samples were exchanged by Au^{+3} ions, resulting in a strain in the crystal structures of TNT-Au^{+3}(C) and TNT-Au^o(C). Moreover, the sample TNT-AuNP(C) was found to be a mixture of nanorods and broken distorted particles as can be seen in SAED pattern which is in agreement to its XRD profile. The presence of Au in TNT-AuNP(C) was also confirmed by the EDS analysis The S_{BET} of TNT-AuNP and TNT-AuNP(C) was found to significantly decrease from 165 to 32 m^2g^{-1} revealing AuNP loading may cause the growth of smaller fragmented particles during calcinations and possessing higher surface area to that of TNT(C).

The observed diverseness in the morphology of TNT-Au^{+3}(C) and TNT-Au^o(C) in comparison to TNT(C) is probably due to induced compression strain (C_{strain}) in their crystal structures. This C_{strain} produced in the crystal structure of TNT after the exchange of Na^+ ions with Au^{+3} ions is believed to inhibit the nucleation growth of TNT during its calcintion at 800 ^{o}C. The formation of smaller particles of size 50-60 nm for TNT-Au^o(C) with more number of boat shaped particles than 65-75 nm of TNT-Au^{+3}(C) can be ascribed to its higher C_{strain} (~25 times) that might have caused inhibition in the nucleation growth during thermal treatment resulting in small size and boat shaped particles. This fact was in-turn confirmed from negligible C_{strain} in the crystal structure of the TNT-AuNP(C), transforming most of TNT particles into nanorods. However, some broken particles of TNT-AuNP(C) are also formed, as the Au-loading at the surface of TNT decreases surface energy and interferes with the crystal growth during calcination, although not calculated here. This work is in agreement with the report of Portai et al. (17), showing the formation of smaller nanoparticles (~ 10 nm) after the post thermal treatment of Rh-impregnated TNT particles.

Although, elemental analysis confirmed the presence of Au but oxidation state of the deposited Au-species over titanate surface was not known. Hence, XPS analysis (Fig. 5) reveals the binding energy of 82.6 eV and 86.8 eV for elemental Au^o characteristic to Au^o ($4f_{7/2}$ and $4f_{5/2}$, respectively) electrons are present in both the Au-photodeposited (TNT-Au^o(C)) and AuNS impregnated (TNT-AuNP(C)) samples as expected. Whereas, the binding energy (83.7 and 87.9 eV) characteristic to Au^{+3} ions are present in TNT-Au^{+3}(C) sample, which are in agreement with the reported (25,26,27) binding energy of Au^{+3} ($4f_{7/2}$ = 83.7 eV and $4f_{5/2}$ = 87.3 eV) and Au^{o} ($4f_{7/2}$ = 82.8 eV and $4f_{5/2}$ = 86.6 eV) oxidation state.

Since, Au loading onto TiO_2 is reported (12,22) to affect the charge recombination process, therefore it was measured (*ESI-fig. 2*) before assessing the PCA of as-prepared catalysts. Fig. 6 showed the average charge recombination time τ_{av} = 68 μs for charge carriers of photoirradiated TNT(C) is ~1.8 times more than τ_{av} = 41 μs for TNT particles that was further increased to the highest τ_{av} = 81 μs after Au-loading and calcination for TNT-Au^{o}(C) catalyst. This increase in τ_{av} is because of the deposits of Au as co-catalyst on the support, acting as a sink for the photogenerated electrons (6,11,22) enhancing the life time of charged species and is in correlation with the results obtained for Au-loaded sodium titanate nanorods in our recent report (23). However, τ_{av} = 67 μs for IMI+TNT-AuNP(C) and τ_{av} = 74 μs for IMI+TNT-Au^{o}(C) was found to be relatively lower than their respective un-adsorbed bare catalyst samples, indicating that the presence of electron withdrawing groups (NO_2 and Cl) in IMI favoring the recombination of excited charge carriers. These results are in accordance to the recent work of Paramaguru et al. (28) where significant quenching in fluorescence intensity was found for pyrene adsorbed TiO_2 possessing substituted electron withdrawing groups in pyrene.

Time course of photocatalytic oxidation of IMI in presence of as-prepared catalysts relative to P25 and the ca. pseudo-first order apparent rate constants are shown in Fig. 7. It is found that no significant change in the amount of IMI was observed when it was irradiated under UV-light in absence of any catalyst, indicating its stability under these experimental conditions.

Among the bare catalysts hollow and porous TNT exhibited the highest photocatalytic activity, whereas Au-loading onto TNT always increases the photocatalytic. The highest photocatalytic activity of TNT is attributed to the collective effect of (i) hollow interior and high specific surface area for better adsorption of the substrate, and (ii) small wall thickness (0.8-1.1 nm) favoring fast diffusion of charge carriers at its surface. The interfacial charge migration is a key factor in deciding the PCA of a catalyst. However, among the various as-prepared bare and Au-loaded catalysts, TNT-Au^o(C) is found to be most photoactive ($k = 8.9\times10^{-3}$ min^{-1}) followed by TNT-Au^o ($k = 5.4\times10^{-3}$ min^{-1}) as compared to the mostly photoactive P25. The high activity (1.6 times) of TNT-Au^o(C) having lower (4 times) S_{BET} than TNT-Au^o can be ascribed to its better crystallinity that may reduces the surface defects acting as recombination sites of excited charge carriers and thus exhibits high photoacativity. This fact is also supported by the time resolve measurements revealing high $\tau_{av} = 81$ µs for TNT-Au^o(C) than $\tau_{av} = 63$ µs for TNT-Au^o sample. Moreover, lower Fermi level position of Au than the conduction band of TiO_2 also favours photo-excited electron transfer from the conduction band of TiO_2 to Au co-catalyst, thus can easily reduce the dissolve O_2 to oxidative superoxide radicals at the catalyst-solution interface. The photoproduced holes in the valance band of TiO_2 can directly oxidize the adsorbed molecule or can produce the oxidative hydroxyl radicals causing further improvement in photocatalytic oxidation of IMI.

The LC chromatographs (*ESI-fig. 3-4*) indicated decrease in peak height of the imidacloprid (retention time $R_t = 2.05$ min) after 180 min of its photooxidation by TNT-Au^o(C) under UV-light irradiation with simultaneous appearance of many new peaks at $R_t = 1.6$, 1.9, 2.3 and 2.5 min. The various intermediate products were identified by LC-MS analysis (Fig. 8) as compound A = 1-(6-chloropyridin-3-yl)methyl)imidazolidin-2-imine (R_t=1.6 min), compound B

= (Z)-N-(1-((6-chloropyridin-3-yl)methyl)-5-hydroxyimidazolidin-2-ylidene)nitramide (R_t = 2.3 min), and compound C = (Z)-N-(1-((6-chloropyridin-3-yl)methyl)-4-hydroxyimidazolidin-2-ylidene)nitramide (R_t = 2.5 min) etc., however the compound D corresponding to R_t = 1.9 in the chromatograph remained unidentified.

Time course graph in Fig. 9 for photomineralization of imidacloprid to CO_2 showed gradual increase in its amount with UV-light irradiation and became the highest (25.7 ppm = 3.1 μmol) in case of TNT-Au^o(C) photocatalyst, showing 34.4 % complete mineralization from 97.2% (48.6 ppm) of its photodegradation, In contrast, only 15.3% (11.5 ppm = 1.38 μmol of CO_2) of mineralization was found from 31.5 ppm (0.71 μmol) of IMI by bare TNT catalyst. This trend indicates incomplete mineralization of IMI due to the formation of heteroatom containing intermediates as identified LC-MS analysis. Thus, it is evident that among all the prepared catalysts and mostly photoactive P25-TiO_2, TNT-Au^o(C) exhibited the highest photocatalytic activity for the complete photomineralization of IMI to CO_2 depending on UV-light irradiation time.

Conclusions

In summary, present work revealed that depending upon thermal treatment, oxidation state and method of Au-loading, sodium titanate nanotubes could be converted to a variety of nanostructures having diverse surface morphology, particles size and shape, crystal structure and composition, which in-turn affects their photocatalytic activity. Thus, it found that sodium titanates after heat treatment at suitable temperature may be useful for preparing more photoactive catalyst than conventional P25-TiO_2 used in many practical applications.

Acknowledgments

The authors acknowledge University Grants Commission and Department of Science and Technology, New Delhi, Government of India for providing financial support. Degussa Corporation, Germany is gratefully acknowledged for the gift of TiO_2 sample.

References:

1. C.K. Lee, C.C. Wang, M.D. Lyu, L.C. Juang, S.S. Liu and S.H. Hung, *J. Colloid Interface Sci.,*2007, **316**, 562–569.
2. J. Yu, H. Yu, B. Chenga and C. Trapalis, *J. Mol. Catal. A Chem.,* 2006, **249**, 135–142.
3. M. Qamar, C.R. Yoon, H.J. Oh, N.H. Lee, K. Park, D.H. Kim, K.S. Lee, W.J. Lee and S.J. Kim, *Catal. Today,* 2008, **131**, 3–14.
4. M. Qamar, C.R. Yoon, H. Jho, D.H. Kim, J.H. Jho, K.S. Lee, W.J. Lee, H.G. Lee and S.J. Kim, *Nanotechnology,* 2006, **17**, 5922–5929.
5. E. Morgado Jr., M.A.S. de-Abreu, O.R.C. Pravia, B.A. Marinkovic, P.M. Jardim, F.C. Rizzo and A.S. Araujo, *Solid State Sci.,* 2006, **8**, 888–900.
6. I.S. Grover, S. Singh and B. Pal, *Appl. Surf. Sci.,* 2013, **280**, 366–372.
7. V. Stengl, S. Bakardjieva, J. Subrt, E. Vecernıkova, L. Szatmary, M. Klementova and V. Balek, *Appl. Catal. B Environ.,* 2005, **63**, 20–30.
8. H. Song, H. Jiang, T. Liu, X. Liu and G. Meng, *Mater. Res. Bull.,* 2007, **42**, 334–344.
9. X. Ding, X.G. Xu, Q. Chen and L.M. Peng, *Nanotechnology,* 2006, **17**, 5423-5427.
10. X. Si, F. Li, L. Sun, F. Xu, S. Liu, J. Zhang, M. Zhu, L.Z. Ouyang, D. Sun and Y.L. Liu, *J. Phys. Chem. C,* 2011, **115**, 9780–9786.
11. M.I. litter, *Appl. Catal. B Environ.,* 1999, **23**, 89–114.
12. J.Y. Tsai, J.H. Chao and C.H. Lin, *J. Mol. Catal. A Chem.,* 2009, **298**, 115–124.
13. D.V. Bavykina, A.A. Lapkinb, P.K. Plucinskib, L.T. Murcianob, J.M. Friedricha and F.C. Walsh, *Top. Catal.,* 2006, **39**, 3–4.
14. J.S. Jang, S. H. Choi, D.H. Kim, J.W. Jang, K.S. Lee and J.S. Lee, *J. Phys. Chem.C,* 2009, **113**, 8990–8996.
15. S. Mandl, G. Thorwarth, B. Stritzker and B. Rauschenbach, *Surf. Coat. Technol.,* 2005, 589-593.
16. M.S.J. Marshall and M.R. Castell, *Phys. Rev. Lett.,* 2009, **160**, 146102–146016.
17. G. Potari, D. Madarasz, L. Nagy, B. Laszlo, A. Sapi, A. Oszko, A. Kukovecz, A. Erdohelyi, Z. Konya, and J. Kiss, *Langmuir,* 2013, **29**, 3061–3072.
18. J. Tang, X. Huang, X. Huang, L. Xiang and Q. Wang, *Environ. Earth Sci.,* 2012, **66**, 441–445.
19. V. Kitsiou, N. Filippidis, D. Mantzavinos and I. Poulios, *Appl. Catal. B Environ.,* 2009,

86, 27–35.

20. W.A. Donald, M.G. Leeming and R.A.J. O-Hair, *Int. J. Mass Spectrom.,* 2012, **316**, 91–99.
21. M.L.D. Arciprete, L.S. Juanes, A.A. Sanz, R. Vicente, A.M. Amat, J.P. Furlong, D.O. Martire and M.C. Gonzalez, *Photochem. Photobiol. Sci.,* 2009, **8**, 1016–1023.
22. R. Kaur and B. Pal, *J. Mol. Catal. A Chem.,* 2012, **355**, 39–43.
23. I.S.Grover, S. Singh and B Pal, *J. Nanosci. Nanotech.,* 2014, doi:10.1166/jnn.2014.9072
24. J.Z. Jin, X. Wang, W. Li, J. Zhang, S. Zhang, X. Guo and Z. Zhang, *Dalton Trans.,* 2003, 3898–3901.
25. F. Yinga, S. Wangb, C.T. Aua and S.Y. Lai, *Gold Bull.,* 2010, **43**, 241-251.
26. X.Z. Li, C. He, N. Graham and Y. Xiong, *J. Appl. Electrochem.*, 2005, **35,** 741–750.
27. A.Z. Jurek, E. Kowalska, J.W. Sobczak,W. Lisowski, B. Ohtani, A. Zaleska, Appl. Catal. B Environ., 2010, **101**, 504–514.
28. G. Paramaguru, R.V. Solomon, S. Jagadeeswari, P. Venuvanalingam and R. Renganathan, *J. Photochem. Photobiol. A: Chem.,* 2013, **271**, 31– 44.

Table and Figure Captions:

Table 1. Description and physic-chemical properties of as-prepared nanostructures.

Fig. 1 XRD pattern of (a) TNT, (b) TNT(C) together with standard reflections (bars), along with TEM images (c) TNT, (d) TNT(C) and SAED patterns (insets).

Fig. 2 XRD pattern (a) TNT-Au^{+3}, (b) TNT-Au^{+3}(C) along with their standard reflections (bars), (c-e) TEM images of TNT-Au^{+3}(C), (f) its corresponding EDS pattern; inset: SAED pattern of TNT-Au^{+3}(C).

Fig. 3 XRD pattern of (a) TNT-Au^{o}, (b) TNT-Au^{o}(C) together with their standard reflections (bars), (c) TEM image of TNT-Au^{o}, (d) its corresponding EDS pattern, (e-f) TEM images of TNT-Au^{o}(C) and its subsequent SAED pattern (inset).

Fig. 4 XRD pattern of (a) TNT-AuNP (b) TNT-AuNP(C), (c-e) TEM images of TNT-AuNP(C) with its corresponding SAED pattern (inset) and (f) its EDS pattern.

Fig. 5 XPS spectrum of Au 4f region of (a)TNT-AuNP(C), (b) TNT-Au^{+3}(C) and (c) TNT-Au^{o}(C).

Fig. 6 Time resolve luminescence decay spectrum for as-prepared samples with average relaxation time.

Fig. 7(a) Photocatalytic degradation of imidacloprid with and without (blank) catalysts and (b) pseudo first order rate constants.

Fig. 8 Schematic representation for structural formulas corresponding to different retention time (R_t) and molecular weights (M.W) of some identified/unidentified compounds.

Fig. 9 Amount of CO_2 produced by photodegradation of imidacloprid at various time intervals with P25 in-comparison to bare and various Au-loaded TNT (before and after calcinations), inset; balanced chemical equation for complete mineralization of imidacloprid

Figures

Fig. 1

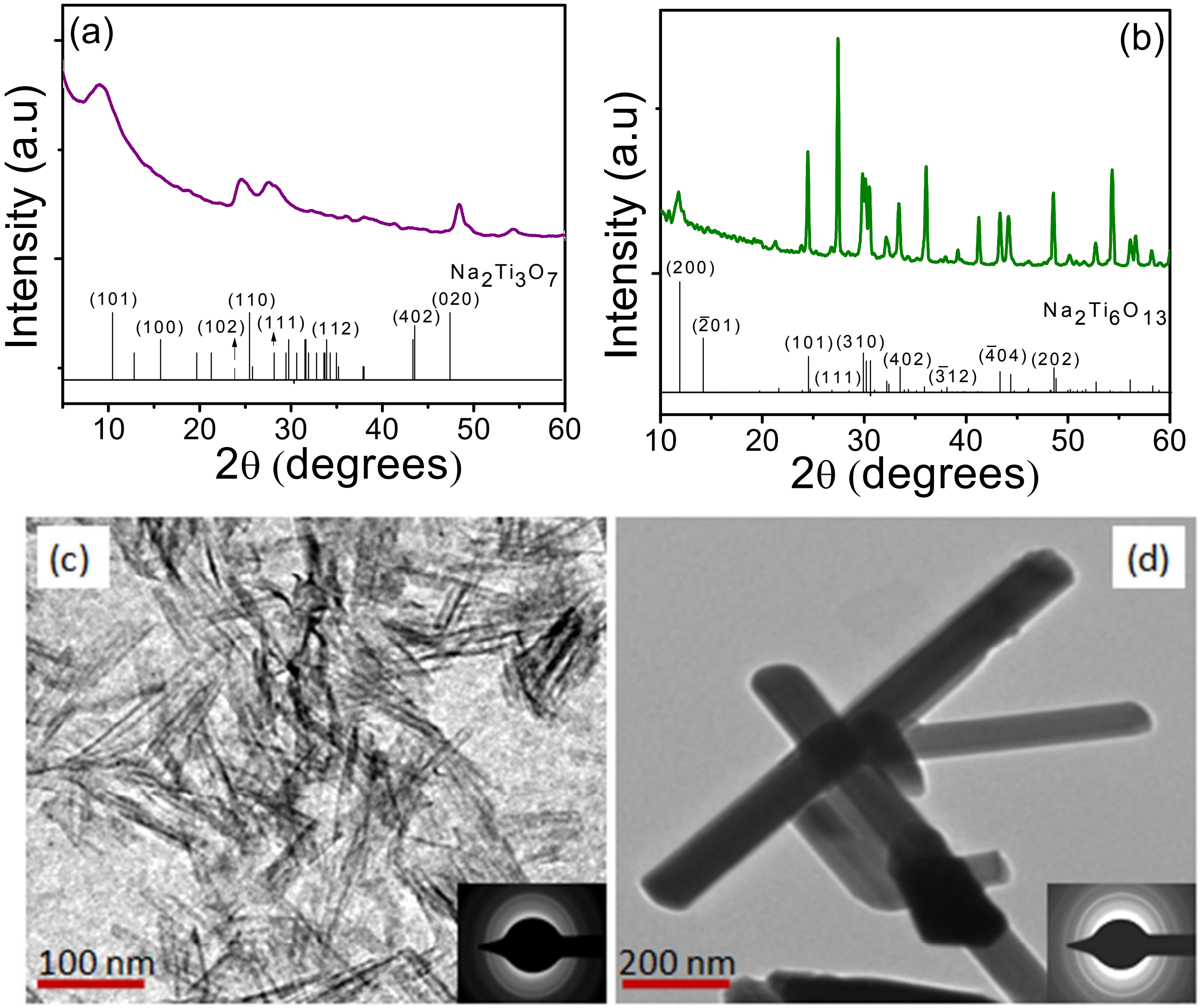

0Fig. 2

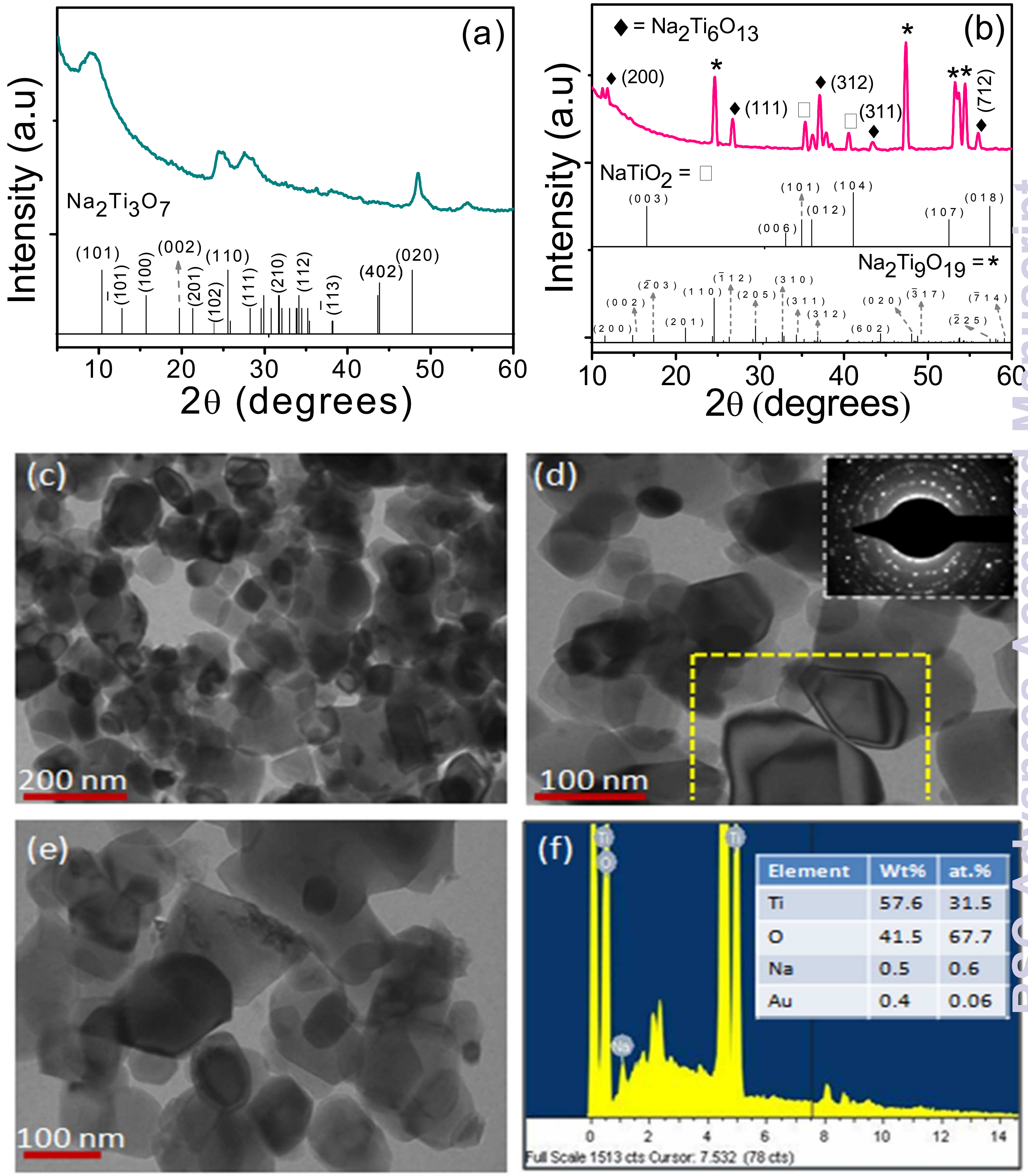

Element	Wt%	at.%
Ti	57.6	31.5
O	41.5	67.7
Na	0.5	0.6
Au	0.4	0.06

Fig. 3

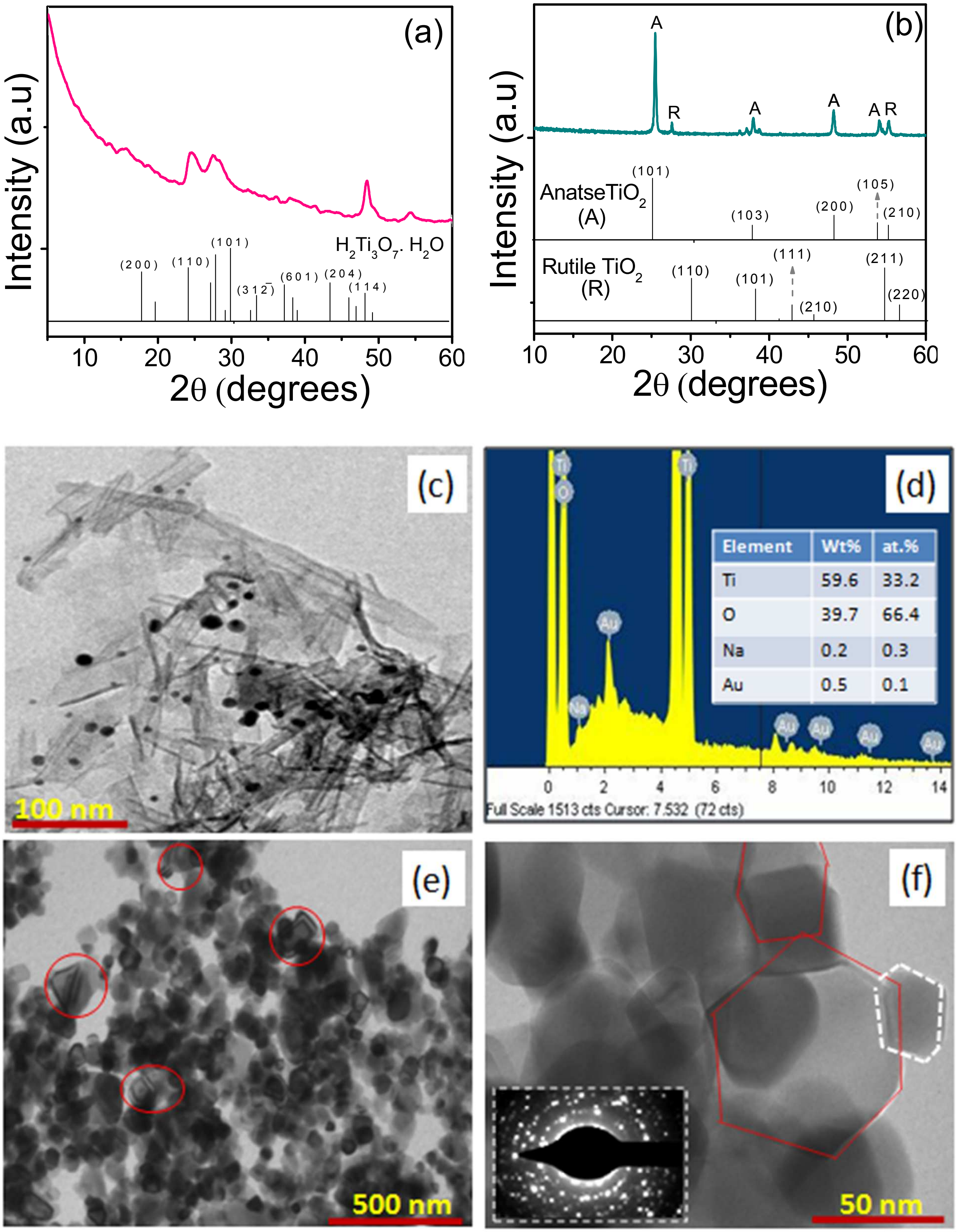

Element	Wt%	at.%
Ti	59.6	33.2
O	39.7	66.4
Na	0.2	0.3
Au	0.5	0.1

Fig. 4

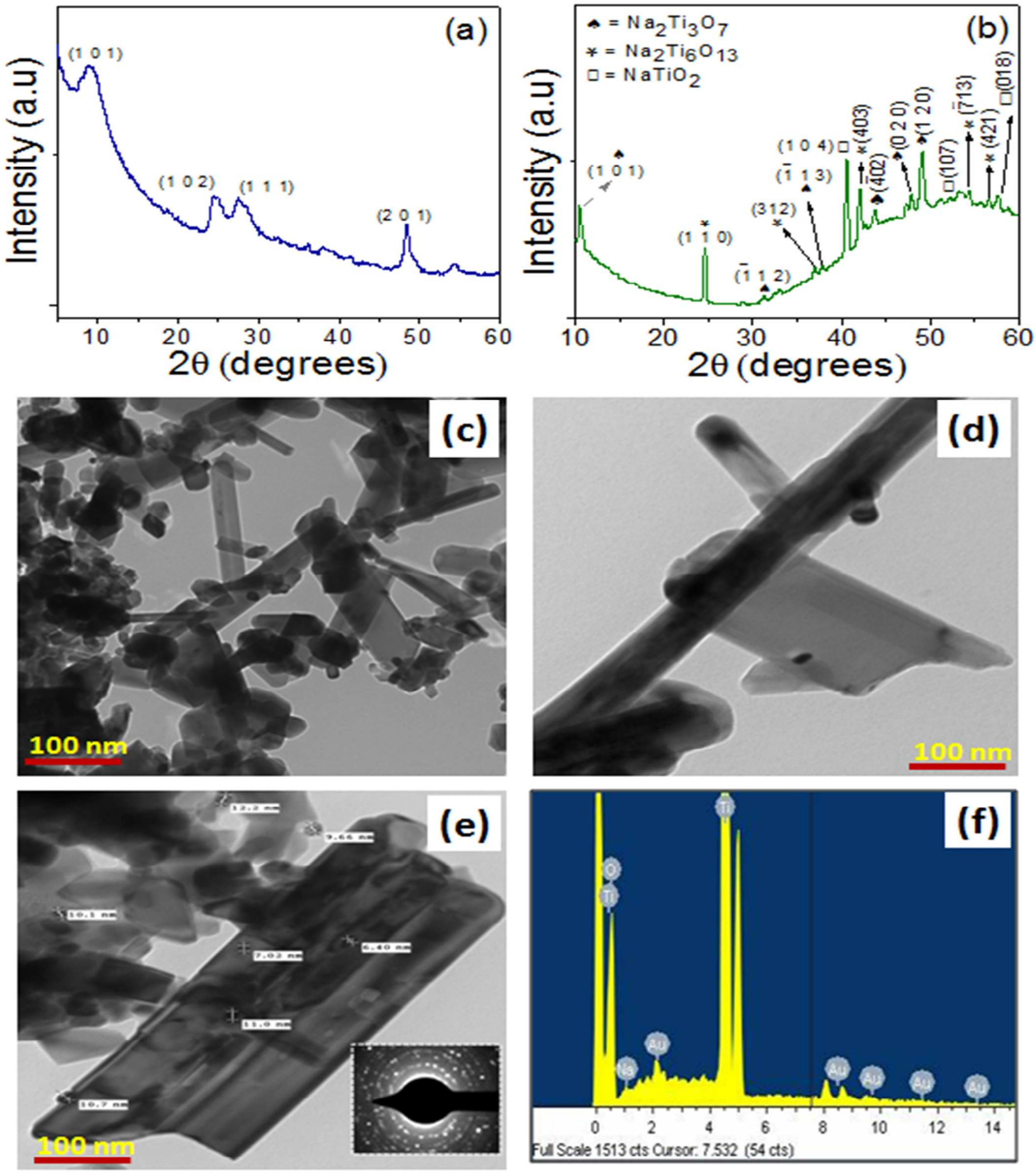
(a)
Intensity (a.u)
(1 0 1)
(1 0 2)
(1 1 1)
(2 0 1)
10
20
30
40
50
60
2θ (degrees)
(b)
♠ = Na2Ti3O7
∗ = Na2Ti6O13
□ = NaTiO2
Intensity (a.u)
(1 0 1)
(1 1 0)
(1̄ 1 2)
(312)
(1̄ 1 3)
(1 0 4)
(403)
(4̄02)
(0 2 0)
(1 2 0)
(107)
(7̄13)
(421)
(018)
10
20
30
40
50
60
2θ (degrees)
(c)
100 nm
(d)
100 nm
(e)
12.2 nm
9.66 nm
10.1 nm
7.02 nm
6.40 nm
11.0 nm
10.7 nm
100 nm
(f)
O
Ti
Na
Au
Ti
Au
Au
Au
Au
0
2
4
6
8
10
12
14
Full Scale 1513 cts Cursor: 7.532 (54 cts)

Fig. 5

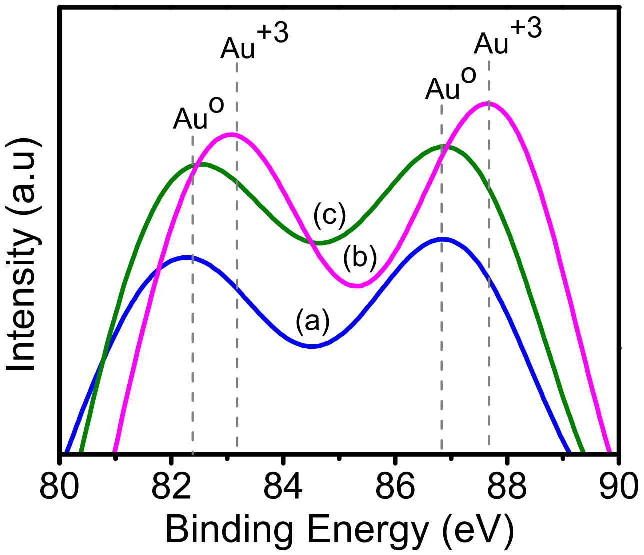

Fig. 6

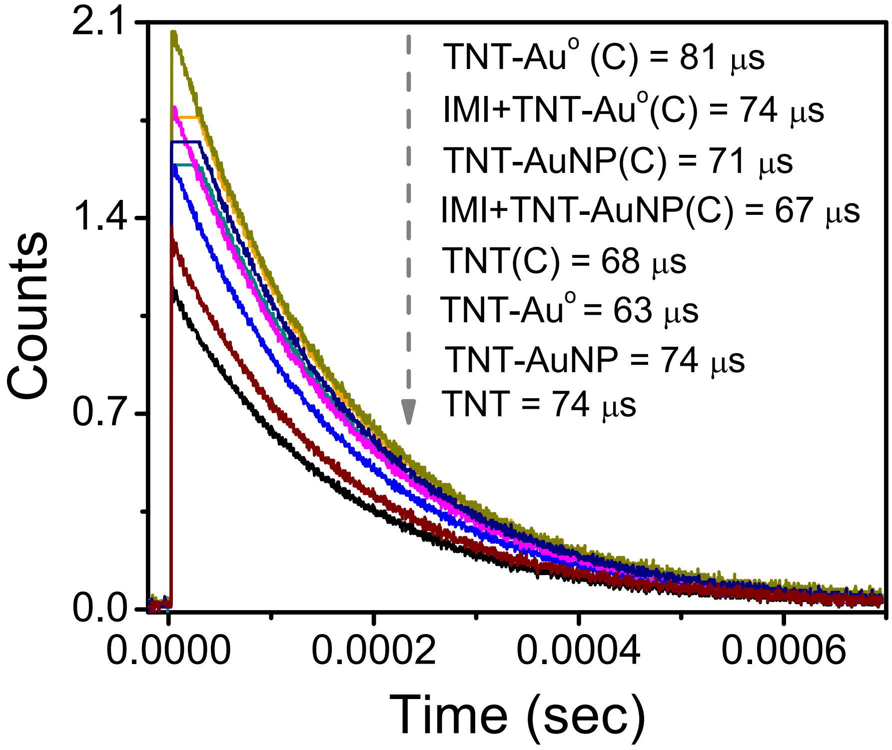

Fig. 7

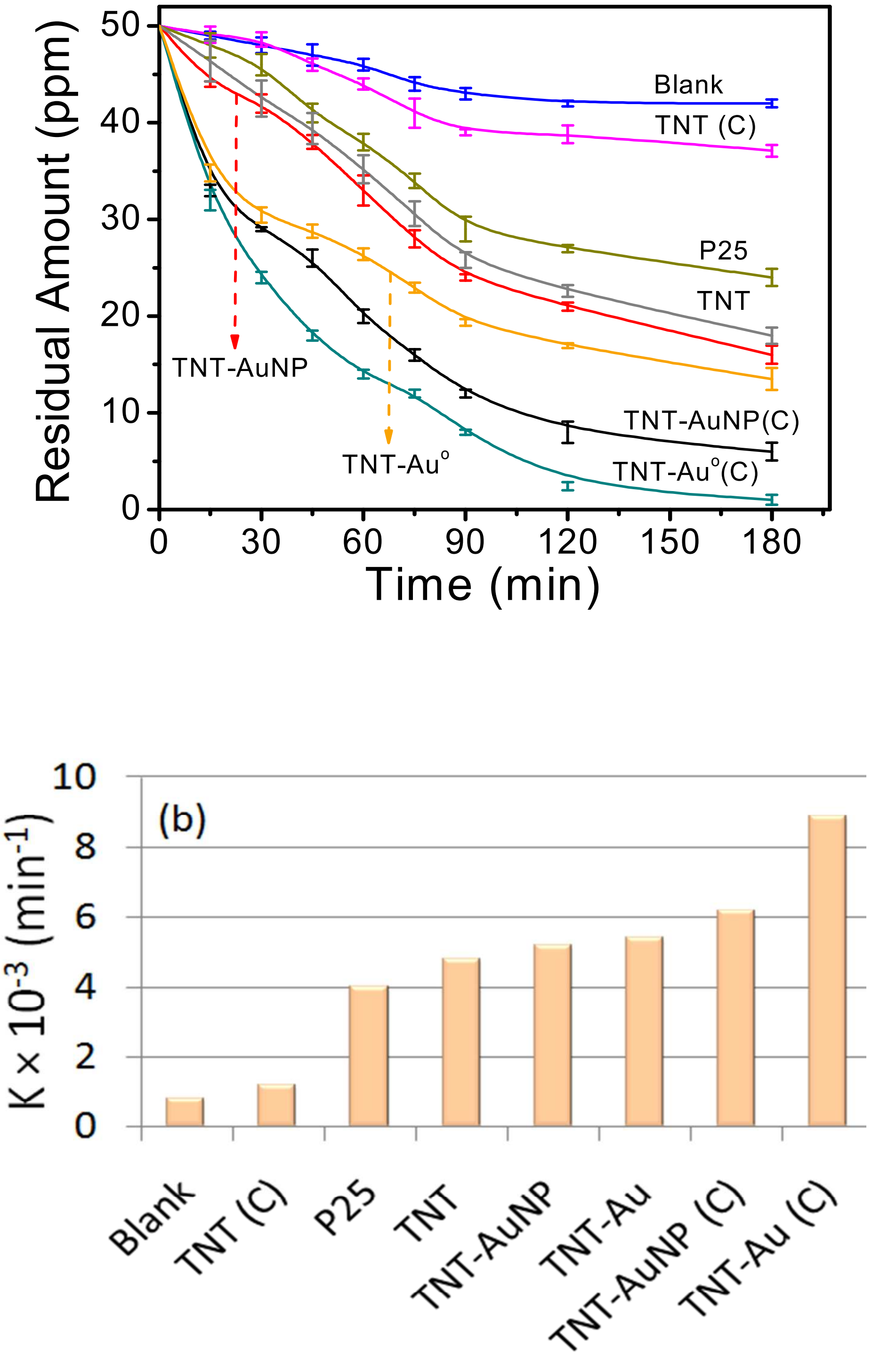
Residual Amount (ppm)
50
40
30
20
10
0
0
30
60
90
120
150
180
Time (min)
Blank
TNT (C)
P25
TNT
TNT-AuNP
TNT-Au°
TNT-AuNP(C)
TNT-Au°(C)
(b)
K × 10-3 (min-1)
10
8
6
4
2
0
Blank
TNT (C)
P25
TNT
TNT-AuNP
TNT-Au
TNT-AuNP (C)
TNT-Au (C)

Fig. 8

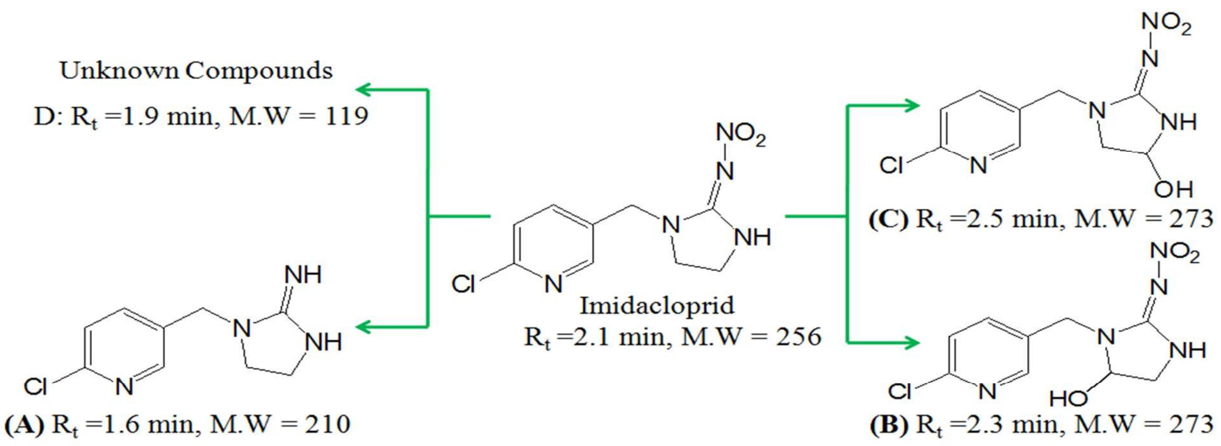
Unknown Compounds
D: R_t =1.9 min, M.W = 119
(A) R_t =1.6 min, M.W = 210
Imidacloprid
R_t =2.1 min, M.W = 256
(C) R_t =2.5 min, M.W = 273
(B) R_t =2.3 min, M.W = 273

Fig. 9

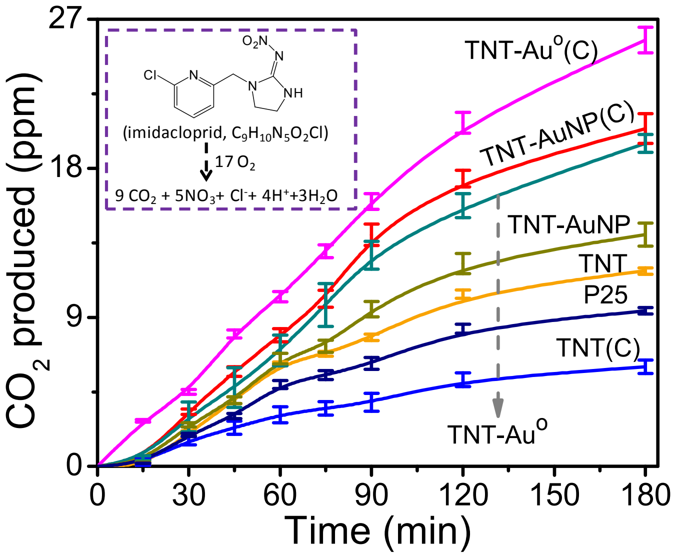
(imidacloprid, $C_9H_{10}N_5O_2Cl$)
17 O_2
9 CO_2 + $5NO_3$+ Cl^-+ $4H^+$+$3H_2O$
TNT-Au^o(C)
TNT-AuNP(C)
TNT-AuNP
TNT
P25
TNT(C)
TNT-Au^O
CO_2 produced (ppm)
Time (min)
0
9
18
27
0
30
60
90
120
150
180

Table 1. Description and physic-chemical properties of as-prepared nanostructures

catalysts	Description	Chemical composition (crystal structure %)	Lattice parameters (Å) Calculated (reported)			EDX analysis Elements (wt%)				Compression Strain
			a	b	c	Na	Ti	O	Au	
TNT	Sodium titanate nanotubes	$Na_2Ti_3O_7$	8.4	3.7	9.0	3.02	57	39	--	7.4×10^{-4}
		(monoclinic, 100%)	(8.5)	(3.8)	(9.1)					
TNT(C)	Sodium titanate nanotubes calcined at 800 °C	$Na_2Ti_6O_{13}$	15.2	3.7	9.1	2.61	58.9	38.4	--	1.5×10^{-4}
		(monoclinic, 100%)	(15.1)	(3.7)	(9.1)					
TNT-Au^{+3}	0.5 wt% Au^{+3} impregnated sodium titanate nanotubes	$Na_2Ti_3O_7$	19.2	3.7	3.0	--	--	--	--	6.9×10^{-3}
		(monoclinic, 100%)	(19.3)	(3.7)	(3.0)					
TNT-Au^{+3} (C)	0.5 wt% Au^{+3} impregnated sodium titanate nanotubes calcined at 800 °C	$Na_2Ti_9O_{19}$	12.2	3.7	15.7	0.15	60.6	38.9	0.3	1.5×10^{-3}
		(monoclinic, 83%)	(12.2)	(3.7)	(15.6)					
		$NaTiO_2$	2.9	3.0	16.2					1.1×10^{-3}
		(rhombohedral, 5%)	(3.0)	(3.0)	(16.2)					
		$Na_2Ti_6O_{13}$	15.2	3.7	9.1					1.4×10^{-3}
		(monoclinic, 12%)	(15.0)	(3.6)	(8.9)					
TNT-Au^{o}(C)	0.5 wt% Au-photodeposited sodium titanate nanotubes calcined at 800 °C	TiO_2 (Anatase, 78%)	12.2	3.7	15.6	0.24	59.5	39.7	0.4	2.4×10^{-2}
			(12.2)	(3.5)	(15.6)					
		TiO_2 (Rutile, 22%)	3.0	3.0	16.2					2.8×10^{-2}
			(2.8)	(2.9)	(16.2)					
TNT-AuNP(C)	0.05 wt% Au nanosphere impregnated sodium titanate nanotubes calcined at 800 °C	$Na_2Ti_6O_{13}$	12.2	3.7	15.6	0.57	57.8	41.5	0.04	0.9×10^{-4}
		(monoclinic, 26%)	(12.2)	(3.7)	(15.6)					
		$NaTiO_2$	3.0	3.0	16.1					0.1×10^{-4}
		(rhombohedral, 46%)	(3.0)	(3.0)	(16.2)					
		$Na_2Ti_3O_7$	19.3	3.7	3.0					0.2×10^{-4}
		(orthorhombic, 28%)	(19.3)	(3.7)	(3.0)					